www.czasopisma.pan.pl PAN POLSKA AKADEMIA NAUK www.journals.pan.pl

Arch. Metall. Mater., Vol. 61 (2016), No 4, p. 2027–2036

DOI: 10.1515/amm-2016-0327

B. HADAŁA*#, Z. MALINOWSKI*, T. TELEJKO*

ANALYSIS OF THE SLAB TEMPERATURE, THERMAL STRESSES AND FRACTURES COMPUTED WITH THE IMPLEMENTATION OF LOCAL AND AVERAGE BOUNDARY CONDITIONS IN THE SECONDARY COOLING ZONES

The numerical simulations of the temperature fields have been accomplished for slab casting made of a low carbon steel. The casting process of slab of 1500 mm in width and 225 mm in height has been modeled. Two types of boundary condition models of heat transfer have been employed in numerical simulations. The heat transfer coefficient in the first boundary condition model was calculated from the formula which takes into account the slab surface temperature and water flow rate in each secondary cooling zone. The second boundary condition model defines the heat transfer coefficient around each water spray nozzle. The temperature fields resulting from the average in zones water flow rate and from the nozzles arrangement have been compared. The thermal stresses and deformations resulted from such temperature field have given higher values of fracture criterion at slab corners.

Keywords: continuous casting of slabs, water spray cooling, local heat transfer coefficient, fracture predictions

1. Introduction

In metallurgical industry water cooling is widely used in continuous casting processes. In the secondary cooling zones water spray cooling is necessary for extracting heat from the solidifying slab. The productivity of the process depends on casting speed and it is a tendency for keeping the casting speed as high as possible. The casting speed is limited mainly by the solidification process which depends on the steel grade and efficiency of the spray cooling system. Designing of the spray nozzles arrangements and controlling the water flow reduces significantly the risk of defects formation. Major issues are concerned with hot tearing and cold cracking. These problems can be solved by the optimization of the cooling system [1]. The optimization of the cooling system can be done using numerical simulation of the slab temperature [2]. The problems in simulation of the slab temperature start with the definition of boundary conditions in the primary cooling zone. The heat transfer between slab and mould is complex and several models can be developed. Depending on the model quality differences in the strand temperature can reach up to 200 K at exit from the mould and vanish at about 5 m below meniscus [3]. Further problems arise in modeling heat transfer boundary conditions in the secondary cooling zones. Hardin at al [4] have calculated the heat transfer coefficient (HTC) from the equation developed by Nozaki at al [5]. This equation defines HTC as a power function of the water flux for spray cooling under film boiling regime only. The HTC has been calculated for the average water flux in zones of cooling. The average in zones HTC has been divided by the correction factor obtained from iterative matching the computed slab surface temperatures with the measured ones. The same method of HTC calculation in spray cooling zones has been implemented by Chaudhuri at al [2]. The two dimensional model of slab temperature makes it possible to automatically adjust the water flow rate in the zones of cooling. The formula for HTC calculation developed by Nozaki at al [5] has been also implemented by Petrus at al [6] and Luo at al [7]. In the two dimensional model of continuous casting process Janik at al [8] have also utilized constant in zones HTC. The formula developed by Nozaki at al [5] takes into account influence of the water flux on HTC but neglects effect of the slab surface temperature. Such HTC models need correction factors in each cooling zone and after that can be implemented only for on line control of the water flow rate in zones of cooling. Essentially better model for water spray cooling has been developed by Hodgson at al [9]. Apart from the water flux the model also takes into account the influence of surface temperature on the HTC and can be implemented under film boiling, transition boiling and nucleate boiling regimes. This model has been utilized by Hadała at al [10] for modeling the temperature field and stress field in the continuously casted strand. However, not only water flux and the surface temperature affect heat transfer during spray cooling. The nozzle type and distance from the nozzle axis (from stagnation point) to a cooling point at the slab surface have also essential influence on the heat flux [11]. Further, Ito at al [12] have shown that the average HTC for the same water flux was 2.8 times lower in the case of the spray nozzle operating at a pressure of 0.7 MPa in comparison to a high pressure of 5 MPa. Hadała [13] has pointed out that the knowledge of HTC as function of the water flux, water pressure and slab surface temperature is essential in simulation of the continuous casting processes.

* AGH UNIVERSITY OF SCIENCE AND TECHNOLOGY, AL. A. MICKIEWICZA 30, 30-059 KRAKOW, POLAND

Corresponding author: beata.hadala@agh.edu.pl

2. Characterization of the modeled continuous casing process

Numerical simulations have been performed for the continuous casting machine which is shown in Fig. 1. The slab 225 mm thick and 1500 mm bright is casted with the speed of 0.9 m/min to the mould having effective length of 800 mm. The caster radius is 10 m with a metallurgical length of 24 m. The slab cross section is shown in Fig. 2 and it has been assumed that the slab corner radius is 16 mm. Further, it has been assumed that the slab bending starts just below the mould along the radius of 10 m and unbending of the slab begins at about 7 m below the mould. The unbending zone ends at about 16.5 m below the meniscus level. Taking into consideration the slab symmetry only a half of the slab cross section has been discredited in the finite element model (FEM) of the slab cooling, Fig. 2. The most important parameters of the slab casting process have been summarized in Table 1.

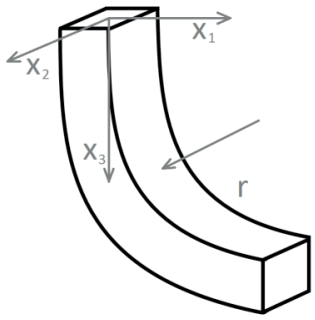

Fig. 1. A schematic drawing of the slab and the coordinate system assumed in FEM model

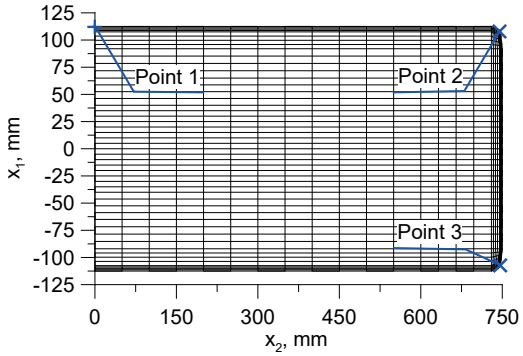

Fig. 2. A half of the slab cross section considered in the FEM model

TABLE 1

Main parameters of the slab casting process considered

Parameter	Unit	Value
Width of the slab	mm	1500
Thickness of the slab	mm	225
Pouring temperature	°C	1530
Casting speed	m/min	0.9
Carbon content of steel	%	0.1
Solidus temperature of steel	°C	1340
Liquidus temperature of steel	°C	1500
Latent heat of solidification of steel	J/m^3	$1.9 \cdot 10^9$
Water spray temperature	°C	20
Ambient temperature	°C	20

The secondary cooling system composed of eight zones has been modeled. The first cooling zone has a length of 0.5 m and is located just below the mould. In this zone the highest water flow rate has been assumed. Zones: 2, 3 and 4 having a length of: 1.1 m, 1.6 m and 2 m, respectively, are located in the bending section. Zones 5 and 6 are located in the unbending section and have a length of 4 m each. The slab unbending ends in zone 7 and the soft reduction take place in the zone 8. The water flow rate in zone 8 is the lowest. The locations of zones and the water flux in each zone have been given in Table 2. The assumed cooling system is typical for casting of slabs and has been derived from data given in [14].

TABLE 2

Parameters of the secondary cooling zones

Zone number	Distance from meniscus	Water pressure assumed in the local HTC model.		Water flux assumed in the average HTC model.	
		Slab width	Slab thickness	Slab width	Slab thickness
	m	MPa	MPa	dm^3/(m^2·s)	dm^3/(m^2·s)
1	0.8-1.3	0.70	0.70	2.5	2.5
2	1.3-2.4	0.60	0	1.3	0
3	2.4-4	0.60	0	0.8	0
4	4-6	0.45	0.60	0.6	0.6
5	6-10	0.45	0.45	0.1	0.1
6	10-14	0.45	0.45	0.08	0.08
7	14-18	0.30	0.30	0.08	0.08
8	18-24	0.20	0.20	0.05	0.05

3. Heat transfer models

Simulation of the slab temperature field in the continuous casting process has been performed with the finite element model developed by Malinowski at all [3]. The slab temperature field has been computed from the FEM solution to the steady-state form of the heat transfer equation:

$$v_x \frac{\partial T}{\partial x} + v_y \frac{\partial T}{\partial y} + v_z \frac{\partial T}{\partial z} = \frac{\lambda}{\rho c}\left(\frac{\partial^2 T}{\partial x^2} + \frac{\partial^2 T}{\partial y^2} + \frac{\partial^2 T}{\partial z^2}\right) + \frac{q_v}{\rho c} \quad (1)$$

where:

T – temperature,
q_v – heat generation rate due to phase changes in steel, W/m^3
c – specific heat, J/(kg·K)
ρ – density, kg/m^3
λ – thermal conductivity, W/(m·K)
v_x, v_y, v_z – velocity field components,
x,y,z – Cartesian coordinates.

The heat transfer boundary conditions and the heat source model employed in the FEM simulations have been described in [3]. For the purpose of the analyses performed in the paper necessary modifications to the heat transfer boundary conditions in the secondary cooling zone have been

introduced. Two models of the heat transfer coefficient (HTC) have been employed in computations. In the first model named as *"average HTC"* the heat transfer coefficient during water spray cooling has been computed from the equation developed by Hodson at all [9].

The average HTC model:

$$\alpha_c = 3.15 \cdot 10^9 \dot{w}^{0.616} \left[700 + \frac{t_s - 700}{exp(0.1t_s - 70) + 1}\right]^{-2.455} \cdot \left[1 - \frac{1}{exp(0.025t_s - 6.25) + 1}\right] \quad (2)$$

where:

t_s – temperature of the slab surface, °C;

$\dot{w}$ – water flux, dm³/(m²·s);

α_c – heat transfer coefficient for water spray cooling, W/(m²·K).

Eq. (2) defines HTC as function of the slab surface temperature and the water flux in a particular water spray zone. The water fluxes assumed in the model at each zone have been given in Table 2. In this case HTC is computed as an average value at each zone and does not depends on the spray nozzles locations and does not take into consideration HTC variation as a distance from the stagnation point (at the nozzle axis) grows [15].

In the second model named as *"local HTC"* which is a modification of Eq. (2) the heat transfer coefficient during water spray cooling is computed from Eq. (3) [13].

The local HTC model:

$$\alpha_c = F_1(p) \cdot F_2(t_s, p) \cdot F_3(t_s) \cdot F_4(r) \quad (3)$$

where:

p – water pressure, MPa

r – distance from the stagnation point, m.

The terms: F_1, F_2 and F_3 in Eq. (3) have the form:

$$F_1(p) = c_1 (p - 0.05)^{-c_2} \quad (4)$$

$$F_2(t_s, p) = 10^6 \left[c_8 + \frac{t_s - c_8}{1 + \exp(t_s \cdot c_4 - c_5)}\right]^{(p \cdot c_3 - 2)} \quad (5)$$

$$F_3(t_s) = \left[1 - \frac{1}{1 + \exp(t_s \cdot c_6 - c_7)}\right] \quad (6)$$

The term F_4 introduces the HTC variation as a distance from the stagnation point grows. The auxiliary variable $r_z = 20r$ has been introduced which divides the water spray zone created by a single nozzle into two subzones in the flowing way:

For $r_z < 1$ the term F_4 is computed from:

$$F_4(r) = \left(1 + |c_{11}| r_s^{|c_{12}|}\right) \exp(-r_s) \quad (7)$$

where:

$$r_s = (20\, r)^{1+|c_9|} \quad (8)$$

For $r_z > 1$ the term F_4 is computed from:

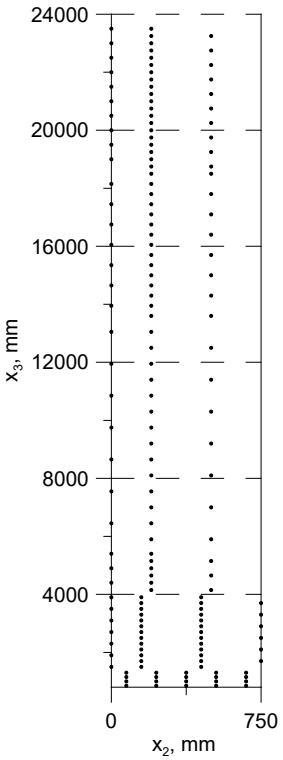

Fig 3. Locations of the water spray nozzles along the slab width and length in the secondary cooling zones

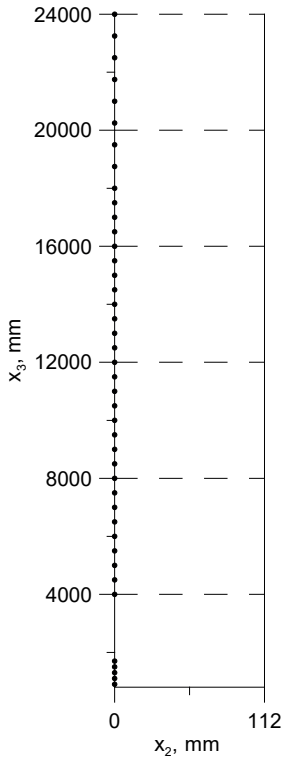

Fig. 4. Locations of the water spray nozzles along the slab thickness and length in the secondary cooling zones

$$F_4(r) = \left(1 + |c_{11}| r_s^{|c_{13} p^{-c_{15}})|}\right) \exp(-r_s) \tag{9}$$

where:

$$r_s = (20\, r)^{|c_{10}(1-p\, c_{14})|} \tag{10}$$

The coefficients c_i in Eq. (4) to Eq. (10) have been determined from the inverse solutions to the water spray cooling of steel plates [13] and are given in Table 3.

The HTC given by Eq. (2) and Eq. (3) define heat transfer due to convection only. The effective HTC can be obtained from the formula:

$$\alpha_e = \alpha_c + \alpha_{ra} \tag{11}$$

The heat transfer due to radiation from the slab surface to surroundings defined by α_{ra} can be computed from the equation given in [3]. In the case of the local HTC model the locations of spray nozzles must be specified. In Fig. 3 and Fig. 4 arrangement of spray nozzles in secondary cooling zones have

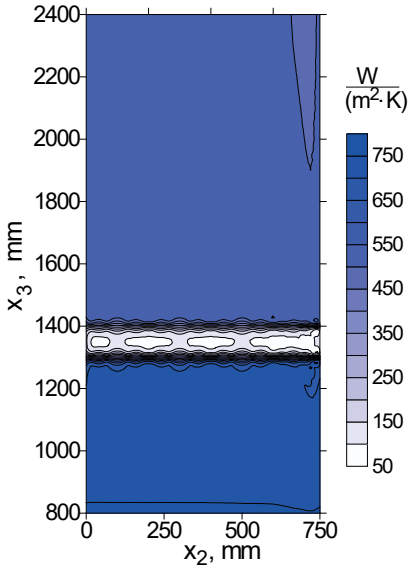

Fig. 5. The HTC distribution at the slab surface in the secondary cooling zones from 0.8 to 2.4 m below meniscus computed from the average HTC model;α_{min} = 42 W/(m2·K); α_{max} = 762 W/(m^2·K)

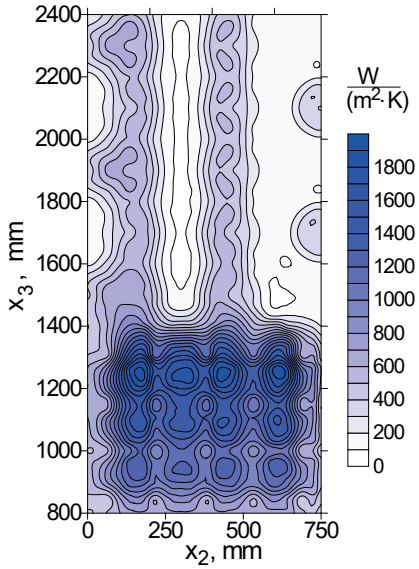

Fig. 6. The HTC distribution at the slab surface in the secondary cooling zones from 0.8 to 2.4 m below meniscus computed from the local HTC model;

α_{min} = 64 W/(m2·K); α_{max} = 1940 W/(m^2·K)

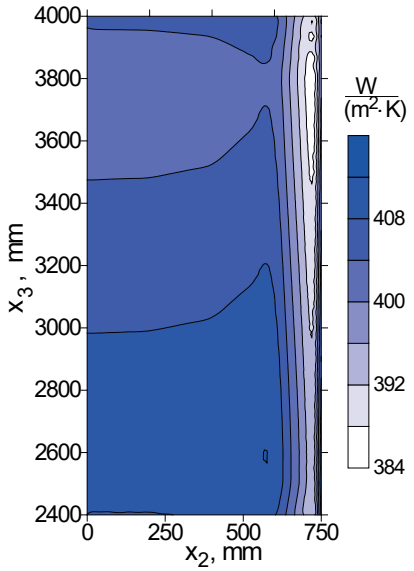

Fig. 7. The HTC distribution at the slab surface in the secondary cooling zones from 2.4 to 4 m below meniscus computed from the average HTC model;

α_{min} = 385 W/(m^2·K); α_{max} = 412 W/(m^2·K)

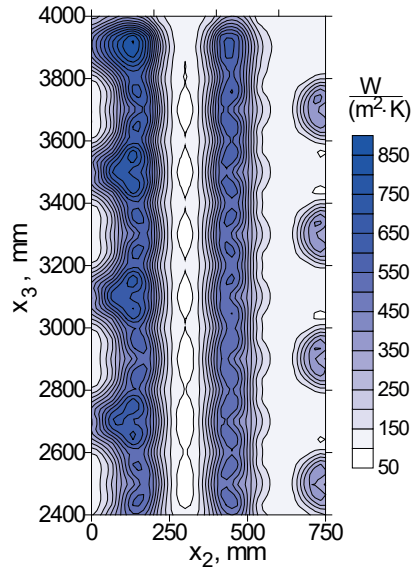

Fig. 8. The HTC distribution at the slab surface in the secondary cooling zones from 2.4 to 4 m below meniscus computed from the local HTC model;

α_{min} = 71 W/(m^2·K); α_{max} = 853 W/(m^2·K)

been shown. The cooling system is composed of 169 nozzles spraying water over the half of the slab width, Fig. 3. On the side surface of the slab in the middle of the slab thickness 42 nozzles have been specified, Fig. 4. The water pressure for nozzles at each cooling zone has been given in Table 2.

The results of HTC computation based on the local and average HTC models have been presented in figures from 5 to 10. The simulation based on the average HTC model has given a total rate of heat extracted from the slab surface of 20.564 MW for the water flow rate given in Table 2. The water pressure in the local HTC model at secondary cooling zones has been chosen at a level which has given a total rate of heat extracted from the slab surface of 21.148 MW. Thus, the difference in the heat extraction rate between models is only 2.8%. The HTC distributions over the slab surface in the first and second cooling zone have been shown in Fig.5 and 6. The average HTC model has given nearly constant HTC along the slab width. Between zone 1 and zone 2 a narrow gap in water spray cooling has been specified in the average HTC model. It has resulted in a sudden drop of HTC to a level of slab cooling in air only. The HTC decreases as the distance from the meniscus grows since the average HTC model takes into account the slab surface temperature. Some variations of HTC near the

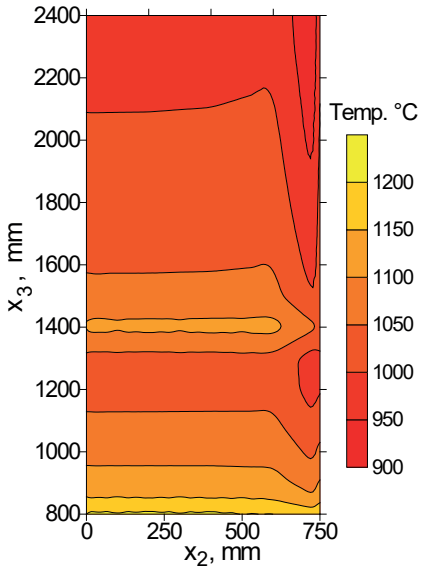

Fig. 9. The temperature distribution at the slab surface in the secondary cooling zones from 0.8 to 2.4 m below meniscus computed from the average HTC model;
t_{min} = 915°C; t_{max} = 1207°C

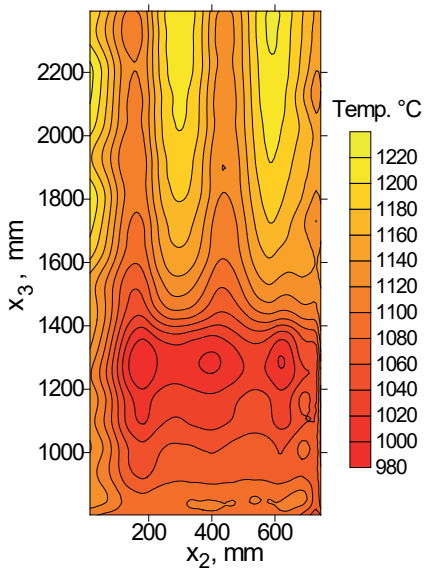

Fig. 10. The temperature distribution at the slab surface in the secondary cooling zones from 0.8 to 2.4 m below meniscus computed from the local HTC model;
t_{min} = 717°C; t_{max} = 1175°C

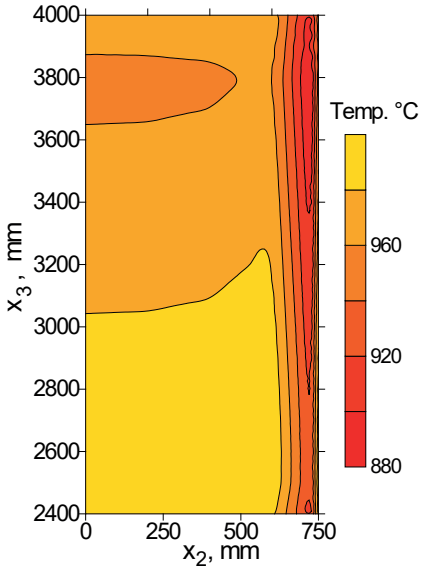

Fig. 11. The temperature distribution at the slab surface in the secondary cooling zones from 2.4 to 4 m below meniscus computed from the average HTC model;
t_{min} = 883°C; t_{max} = 998°C

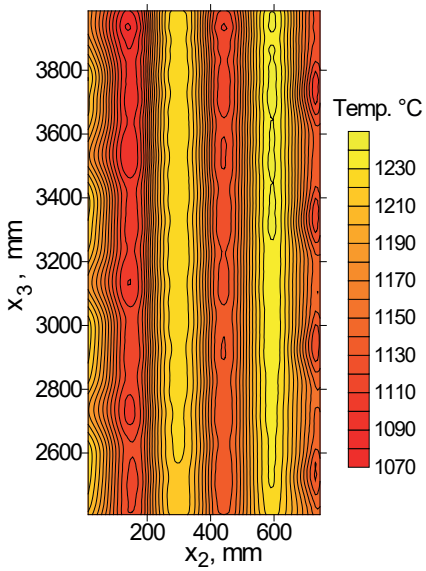

Fig. 12. The temperature distribution at the slab surface in the secondary cooling zones from 2.4 to 4 m below meniscus computed from the local HTC model;
t_{min} = 746°C; t_{max} = 1225°C

slab edge are also visible and are due to lower slab surface temperature. The average HTC model has given a HTC maximum of 760 W/(m^2·K) in the first cooling zone. The local HTC model has resulted in highly heterogeneous HTC distribution in the first and second cooling zone. A maximum HTC of 1940 W/(m^2·K) has been obtained in the first cooling zone. Between nozzles, where the water flow vanishes, the HTC drops to a level of radiation. The locations of nozzles are also visible as the HTC maxima in Fig. 6.

In the third cooling zone the average HTC model has given HTC values in the range from 385 to 412 W/(m^2·K) due to the slab surface temperature changes only, Fig. 7. In the third cooling zone the local HTC model has given the HTC variations resulting from nozzles arrangement, water flow and surface temperature, Fig. 8. The HTC values vary in this zone from 71 to 853 W/(m^2·K).

4. The slab temperature field simulations

The average and the local HTC models result in the slab surface temperature variations. In the first and the second cooling zones the slab surface temperature obtained from the average HTC model varies from 915 to 1207°C, Fig. 9. The local HTC model has given the surface temperatures from 717 to 1175°C, Fig. 10. In the third cooling zone the average HTC model has given the slab surface temperature in the range from 883 to 998°C, Fig. 11. The implementation of the local HTC model has resulted in the slab surface temperatures from 746 to 1225°C, Fig. 12. The maximum difference in the surface temperature computed from the average HTC model in the first and the second cooling zone is of 290°C, while the local HTC model has given a temperature difference of 460°C. The slab surface temperature differences obtained from the local HTC model in the third zone are even higher at a level of 480°C. The temperature variations along the slab at points: P_1, P_2 and P_3 have been presented in Fig. 13 and 14.

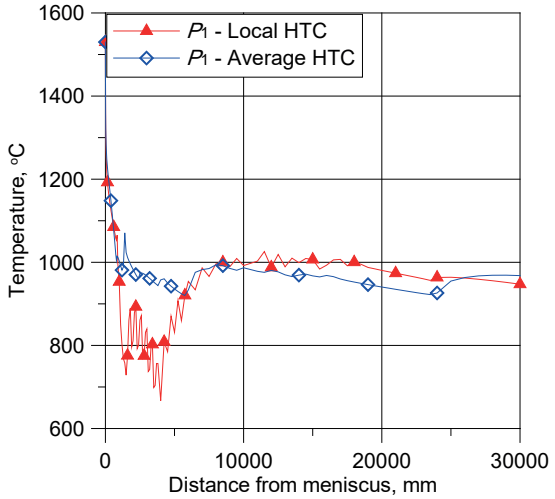

Fig. 13. The temperature variations at the slab surface in the middle of the slab width obtained from the average and local boundary condition models

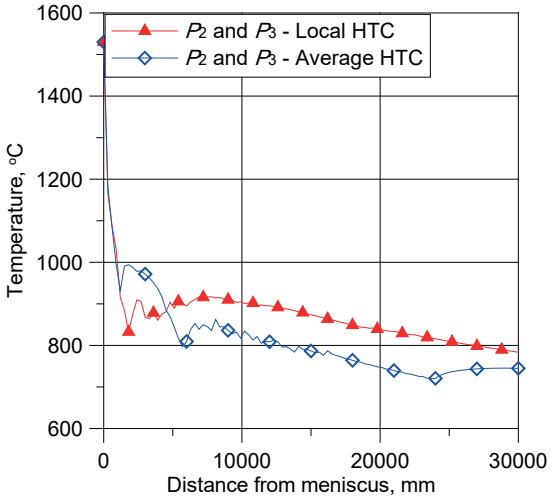

Fig. 14. The temperature variations at the slab corners obtained from the average and local boundary condition models

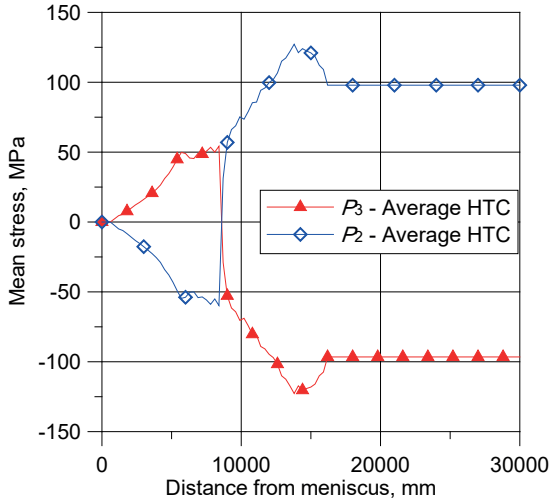

Fig. 15. The mean stress variations at the slab corners caused by slab bending obtained from the average HTC model

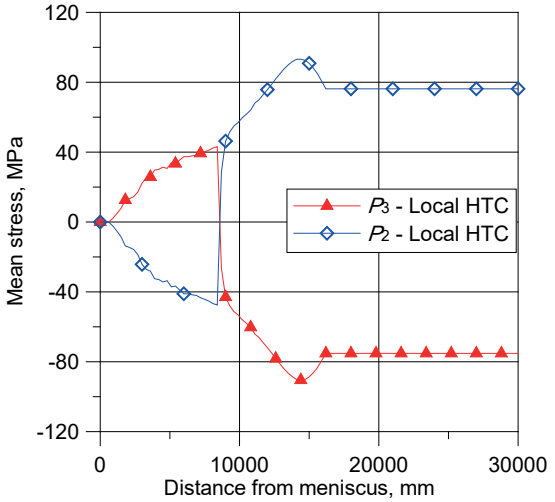

Fig. 16. The mean stress variations at the slab corners caused by slab bending obtained from the local HTC model

The location of points is shown in Fig. 2. Point P_1 is located in the middle of the slab width at the slab surface. Points P_2 and P_3 are located at the upper and lower corners of the slab. At the center of the slab surface the average HTC model has given essentially higher temperatures in the first three cooling zones. The implementation of the local HTC model has resulted in the slab surface temperature fluctuations and essential temperature drop. These effects have been caused by the transition boiling under high water pressure.

The temperature variations at the slab corners have been presented in Fig. 15. The average HTC model has given higher corner temperatures in the first three cooling zones and higher temperatures above 4 m from the meniscus level. The local HTC model has given higher corner temperatures above 4 m from the meniscus because this model takes into account locations of the spray nozzles. In the zones of cooling from 4 to 8 the spray nozzles are not located near the slab corners. This effect cannot be achieved with the average HTC model.

5. Modeling of thermal stresses and fractures

The elastic-plastic finite element model has been used for computing the stress and strain fields in the slab [10]. The strain rate and stress fields resulting from slab bending and unbending is computed as part of the mechanical model. The thermomechanical properties of the deformed material as functions of temperature for the low carbon steel having 0.1% of carbon content have been given in [10]. Mean stress distributions at slab corners resulting from slab deformations along the arc of casting machine have been presented in Fig. 15 and 16. The results obtained from the temperature field computed for average and local HTC models are similar. The heat transfer model does not have direct influence on the deformation field resulting from slab bending and unbending. This part of slab deformation depends mainly on the arc of casing machine. In computations the arc of 10 m has been assumed. The slab bending starts just below the mould and the mean stress is compressive at inner corner of and tensile

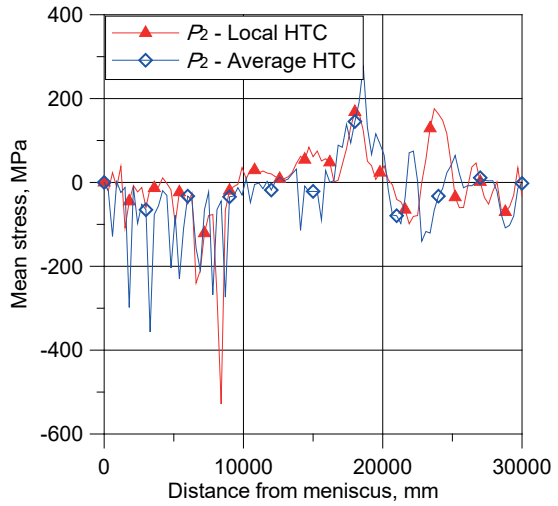

Fig. 17. The mean stress variations at the slab inner corner obtained from the average and local HTC models

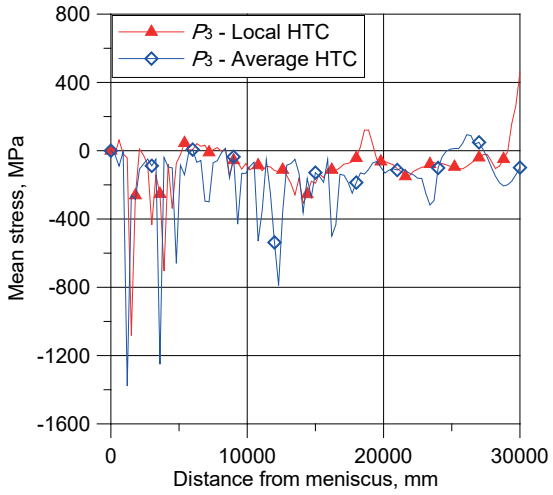

Fig. 18. The mean stress variations at the slab outer corner obtained from the average and local HTC models

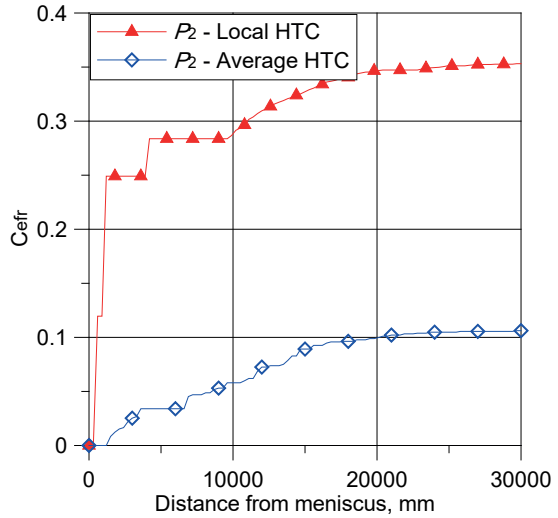

Fig. 19. The crack criterion change at the slab inner corner obtained from the average and local HTC models

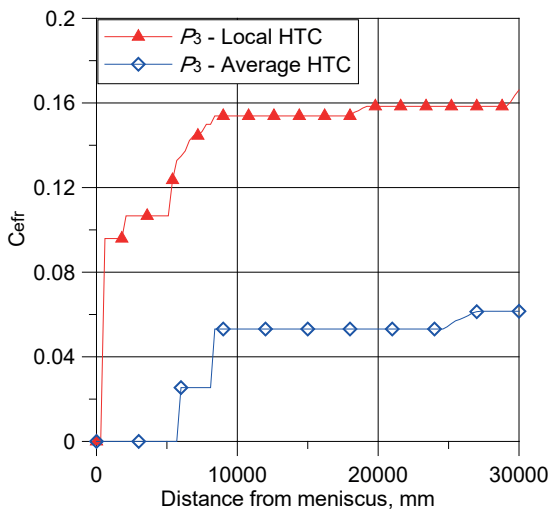

Fig. 20. The crack criterion change at the slab outer corner obtained from the average and local HTC models

at outer corner of the slab. The mean stress changes sign from positive to negative and from negative to positive as the slab enters the unbending zone. The mean stress values obtained from local and average HTC models differ slightly due to the flow stress which depends on temperature. The local HTC model has given higher temperature at slab corners and it has resulted in the lower flow stress and mean stress values. The heat transfer model has main influence on the deformation and stress fields resulting from thermal dilatation and phase transformations in steel. The thermal expansion coefficient as function of temperature for the considered steel has been given in [10]. The mean stress distributions at slab corners resulting from slab deformation at the arc of caster and thermal effects have been shown in Fig. 17 and Fig. 18.

The means stress distributions at the slab corners shown in Fig. 17 and Fig. 18 vary significantly along the slab length. Comparing the mean stress values caused by slab bending with the results presented in these figures it can be concluded that thermal effects have much higher influence on the mean stress. However, it is practically impossible to draw conclusions concerning the risk of fracture occurrence on mean stress distributions only.

For the present study the simple fracture criterion has been chosen. The effective strain has been calculated along the particle path. The fracture criterion C_{efr} value has been defined as:

$$C_{efr} = \int_0^t \dot{\bar{\varepsilon}}\, dt \qquad \text{for} \quad \sigma_m > 0 \tag{12}$$

where: $\dot{\bar{\varepsilon}}$ – effective strain rate, σ_m – mean stress, t – time necessary to reach a particular point at the particle path.

The strain criterion (12) is simple in form and can be directly compared with the results of tensile tests obtained for a very similar grade of steel by Zhang at all [17]. The hot ductility tensile tests published in [17] has given a lowest effective strain at fracture of ε_f=0.22 at temperature of 785°C. At temperature of 900°C the effective strain at fracture was about ε_f=0.51. Thus fractures of slab corners are possible at points for which the temperature drops to about 800°C and the fracture criterion C_{efr} reaches a value about 0.22. In Fig. 19 and 20 the distributions of the fracture criterion C_{efr} values at slab corners have been presented. The fracture criterion values resulted from the temperature field obtained for the average HTC model are essentially lower than 0.22 along the slab length. The fracture criterion values calculated for the stress and strain fields obtained from the temperature field computed with the use of the local HTC model are essentially higher. At point P_3 the values of fracture criterion are below the ductility limit but at point P_2 C_{efr} has reached 0.25 at the distance of 5m below meniscus. At that distance the corners temperatures approaches 800°C and fractures are possible.

TABLE 3

Coefficients of the local HTC model

c_1=48.2290	c_4=-1.78380	c_7=6.5984	c_{10}=1.8512	c_{13}=0.67339
c_2=0.17352	c_5=11.79600	c_8=4461.5	c_{11}=2.7160	c_{14}=0.69445
c_3=0.51745	c_6=0.058305	c_9=2.4744	c_{12}=1.1513	c_{15}=0.21459

6. Conclusions

In simulations of the temperature fields of the continuously casted slabs determination of the heat transfer boundary conditions is a complex issue and has essential influence on the results of computations. The majority of heat transfer models available in literature defines average heat flux or heat transfer coefficient in secondary cooling zones. The boundary conditions which depend on water flux only are suitable for on line models controlling the water flow in zones of cooling. Modeling of local phenomena such as fracture requires heat transfer boundary conditions which depend on water flux distribution. It has been shown that implementation of local heat transfer boundary conditions which take into account locations of nozzles results in highly non-uniform temperature of the slab surface. It gives the possibility of more realistic modeling of thermal stresses. Due to temperature variations higher values of fracture criterion at slab corners have been obtained for the local boundary condition model which reflects the nozzles arrangement in the heat transfer.

Acknowledgements

Scientific study financed from the regular activity of the Faculty of Metals Engineering and Industrial Computer Science of AGH University of Science and Technology, Work no. 11.11.110.226

REFERENCES

[1] J. Sengupta, B.G. Thomas, M.A. Wells, The use of water cooling during the continuous casting of steel and aluminum alloys, Metallurgical and Materials Transaction A **36A**, 187-204 (2005).

[2] S. Chaudhuri, R.K. Singh, K. Patwari, S. Majumdar, A.K. Ray, A.K. Prasad Singh, N. Neogi, Design and implementation of an automated secondary cooling system for the continuous casting of billets, ISA Transactions **49**, 121-129 (2010).

[3] Z. Malinowski, T. Telejko, B. Hadała, Influence of heat transfer boundary conditions on the temperature field of the continuous casting ingot, Archives of Metallurgy and Materials **57**, 325-331 (2012).

[4] R.A. Hardin, K. Liu, A. Kapoor, Ch. Beckermann, A transient simulation and dynamic spray cooling control model for continuous steel casting, Metallurgical and Materials Transactions B **34B**, 297-306 (2003).

[5] T. Nozaki, J.I. Matsuno, K. Murata, H. Ooi, and M. Kodama, Trans. Iron Steel Inst. Jpn. **18**, 330-338 (1978).

[6] B. Petrus, K. Zheng, X. Zhou, B. G. Thomas, J. Bentsman, Real-time, model-based spray-cooling control system for steel continuous casting, Metallurgical and Materials Transactions B **42B**, 87-103 (2011).

[7] W. Luo, B. Yan, Y. X. Xiong, G. H. Wen, H. L. Xu, Improvement to secondary cooling scheme for beam blank continuous casting, Ironmaking and Steelmaking **39**, 125-132 (2012).

[8] M. Janik, H. Dyja, S. Berski, G. Banaszek, Two-dimensional thermomechanical analysis of continuous casting process, Journal of Materials Processing Technology **153-154**,

578-582 (2004).

[9] P. D. Hodgson, K. M. Browne, D.C. Collinson, T. T. Pham, R. K. Gibbs, A mathematical model to simulate the thermo-mechanical processing of steel, Proceedings of 3rd International Seminar of the International Federation for Heat Treatment and Surface Engineering, Melbourne pp. 139-159, 1991.

[10] B. Hadała, A. Cebo-Rudnicka, Z. Malinowski, A. Gołdasz, The influence of thermal stresses and strand bending on surface defects formation in continuously cast strands, Archives of Metallurgy and Materials **56**, 367-377 (2011).

[11] D. Li, M.A. Wells, Effect of water flow rate, water temperature, nozzle size and nozzle stand-off distance on the boiling water heat transfer of AISI 316 stainless steel plate, Canadian Metallurgical Quarterly **44**, 59-70 (2005).

[12] Y. Ito, T. Murai, Y. Miki, M. Mitsuzono, T. Goto, Development of hard secondary cooling by high-pressure water spray in continuous casting, ISIJ International **51**, 1454-1460 (2011).

[13] B. Hadała, Validation of the boundary condition models and boundary condition identification for water spray cooling of steel, 2016 Wydawnictwa AGH, Kraków,

[14] J. Falkus, Modelowanie procesu ciągłego odlewania stali, 2012 PIB, Radom

[15] Z. Malinowski, A. Cebo-Rudnicka, T. Telejko, B. Hadała, A. Szajding, Inverse method implementation to heat transfer coefficient determination over the plate cooled by water spray, Inverse Problems in Science and Engineering **23**, 518-556 (2015).

[16] B. Hadała, A. Cebo-Rudnicka, Z. Malinowski, A. Gołdasz, The influence of thermal stresses and strand bending on surface defects formation in continuously cast strands, Archives of Metallurgy and Materials **56**, 367-377 (2011).

[17] L. Zhang, X. Yang, S. Li, M. Li, W. Ma, Control of Transverse Corner Cracks on Low-Carbon Steel Slabs, The Minerals, Metals & Materials Society, (2014), **66**, 1711-1720 (2014).